ELSEVIER

International Journal of Solids and Structures 41 (2004) 3891–3904

INTERNATIONAL JOURNAL OF SOLIDS and STRUCTURES

www.elsevier.com/locate/ijsolstr

Development of pile-up during spherical indentation of elastic–plastic solids

B. Taljat [a,b], G.M. Pharr [c,d,*]

[a] *STEEL Group, Via Lazio 1/B, 31045 Motta di Livenza (TV), Italy*

[b] *Technology and Consulting Center, 1000 Litostrojska 40, Ljubljana, Slovenia*

[c] *Department of Materials Science and Engineering, The University of Tennessee, 434 Dougherty Engineering Building, Knoxville, TN 37996-2200, USA*

[d] *Oak Ridge National Laboratory, Metals and Ceramics Division, P.O. Box 2008, Oak Ridge, TN 37831, USA*

Received 7 August 2003; received in revised form 11 February 2004

Available online 24 March 2004

Abstract

Finite element modeling has been used to study the development of pile-up during indentation with a rigid sphere as it relates to the measurement of mechanical properties by load and depth sensing indentation. A wide range of materials with different elastic moduli, yield stresses, strain-hardening exponents, and friction coefficients were examined. Results show that during a significant portion of the spherical indentation process, the amount of pile-up cannot be related solely to the strain-hardening exponent, as is often assumed. Rather, after initially sinking-in at small depths of penetration, the pile-up for many materials evolves and increases gradually as the indenter is driven into the material. Even when deformation enters the fully developed plastic stage, the pile-up geometry continues to change in manner that can significantly affect the contact area. It is also shown that contact friction affects the pile-up geometry, and that the pile-up heights before and after the indenter is unloaded can be quite different. Implications for the measurement of mechanical properties by load and depth sensing indentation methods are discussed.

Keywords: Spherical; Indentation; Finite element; Elastic–plastic solids

1. Introduction

In measuring material properties by load and depth sensing indentation methods, it is essential that the contact geometry be established precisely since analysis procedures used to determine properties like the hardness, H, and elastic modulus, E, rely heavily on an accurate determination of the contact area (Oliver and Pharr, 1992; Pharr, 1998). However, measurement of the contact area from indentation load-depth

* Corresponding author. Address: Department of Materials Science and Engineering, The University of Tennessee, 434 Dougherty Engineering Building, Knoxville, TN 37996-2200, USA. Tel.: +1-865-974-8202; fax: +1-865-974-4115.

E-mail address: pharr@utk.edu (G.M. Pharr).

0020-7683/$ - see front matter © 2004 Elsevier Ltd. All rights reserved.
doi:10.1016/j.ijsolstr.2004.02.033

data is not necessarily a straightforward process, as it depends on the amount pile-up or sink-in of material around the contact impression. Bolshakov and Pharr (1998) examined the significance of pile-up for rigid conical indenters and found that if pile-up is neglected, the true contact area can be underestimated by as much as 60%, leading to similar errors in calculated material properties. Thus, a complete understanding indentation of pile-up and sink-in is crucial to making accurate property measurements.

For conical and pyramidal indenters, the amount of pile-up or sink-in is not a function of the indentation depth. For spherical indenters, on the other hand, the pile-up and sink-in geometry may change significantly during indentation by virtue of the transition from purely elastic deformation at small depths to plastically dominated behavior at large depths. The contact geometry for spherical indentation is illustrated in Fig. 1, which shows a rigid sphere of radius R driven into a material by a force P to a penetration depth h. The right-hand side of the figure shows the behavior when material sinks-in and the left-hand side when it piles-up. Because of sink-in and pile-up, the contact depth, h_c, which is the actual depth along which contact is made between the specimen and indenter, may differ from the total indenter penetration depth, h. In addition, there will be two contact radii of interest: the actual radius of contact, a_c, and the surface contact radius, a, defined by the intersection of the indenter with the original undeformed surface. The surface contact radius is that which would be determined from the measured depth of penetration if there were no pile-up or sink-in. The amount of pile-up or sink-in can be characterized by the height, s, of the pile-up or sink-in relative to the undeformed surface, where $s > 0$ for pile-up and $s < 0$ for sink-in. The parameter β, which is related to the amount of strain induced by the indenter and therefore changes with depth of penetration, is the angle between the tangent line to the contact at its periphery and the undeformed surface. Note that when the load is removed, the contact impression may partially or totally recover by elastic processes.

It is useful to consider the pile-up and sink-in behavior during spherical indentation in terms of the deformation regimes suggested by Johnson (1985). Letting p_m be the mean pressure under the indenter and σ_y the yield stress, Johnson found that there is a unique correlation between $E/\sigma_y \tan\beta$, the ratio of the strain imposed by the indenter ($\tan\beta$) to the elastic strain the material can accommodate before yielding (σ_y/E), and the normalized contact pressure, p_m/σ_y. The parameter p_m/σ_y is also called the "constraint factor" because it characterizes the extent to which elastic material surrounding the contact impression inhibits yielding and plastic deformation during indentation. Johnson identified three discernible indentation regimes based on observed relationships between p_m/σ_y and $E/\sigma_y \tan\beta$: (1) *the elastic regime* at small loads and depths, where contact is strictly elastic and there is a linear increase of p_m/σ_y with $E/\sigma_y \tan\beta$; (2) *the elastic–plastic transition regime*, in which plasticity commences beneath the surface and p_m/σ_y increases linearly with $\log(E/\sigma_y \tan\beta)$; and (3) *the fully plastic regime*, in which plasticity escapes to the free surface and the release of constraint causes p_m/σ_y to stabilize at a relatively constant value of about 3.

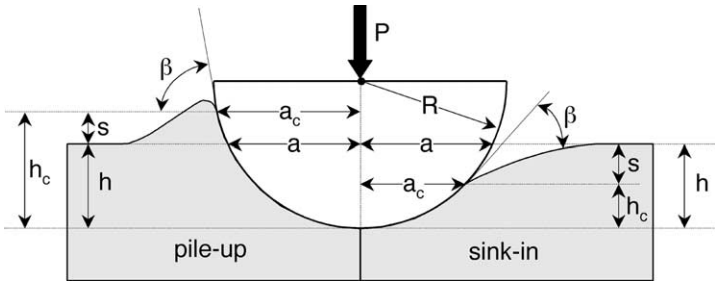

Fig. 1. Spherical indentation contact geometry. Important parameters are: indenter radius, R; load, P; depth of penetration, h; contact depth, h_c; true contact radius, a_c; surface contact radius, a; pile-up/sink-in height, s.

The behavior of spherical indentation in the elastic regime is well described by the theory of Hertz (1896). For this strictly elastic deformation, the contact periphery sinks-in by an amount exactly equal to half the total depth of penetration. Thus, both the sink-in of the surface at the contact edge, s, and the contact depth, h_c, are equal to $h/2$ (see Fig. 1). When the contact is unloaded, the contact fully recovers and no residual hardness impression remains. At the other extreme, indentation at large depths in the fully plastic regime causes a permanent hardness impression to be formed, but whether the indentation piles-up or sinks-in depends on the strain-hardening characteristics of the material (Tabor, 1951; Hill et al., 1989; Biwa and Storakers, 1995; Norbury and Samuel, 1928; Matthews, 1980; Field and Swain, 1995; Francis, 1976; O'Neil, 1944). Hill et al. provided an analysis based on deformation theory to examine the limiting behavior for plastic materials exhibiting simple power-law hardening of the form $\sigma = K\varepsilon^n$, where σ is the stress, ε is the strain, K is the strain hardening coefficient, and n is the strain hardening exponent. They found that the degree of pile-up or sink-in is a unique function of n that can be conveniently described through a parameter $c^2 = a_c^2/2Rh$. In the limit of small penetration depths, c^2 has a simple physical interpretation: it is the ratio of the depth along which contact is made to the total depth of penetration, h_c/h. Thus, $c^2 < 1$ implies that material sinks-in, while $c^2 > 1$ means that material piles up. Hill et al. found that the relationship between n and c^2 can be approximated as

$$c^2 = \frac{5}{2}\left(\frac{2-n}{4+n}\right). \tag{1}$$

Later, Biwa and Storakers (1995) reexamined the problem using the flow theory of plasticity and obtained qualitatively similar results, although with slightly different numerical predictions for the extent and form of the pile-up and sink-in.

Fig. 2 compares the predictions of the theoretical analyses of Hill et al. and Biwa and Storakers to experimental data for a variety of metals obtained by Norbury and Samuel (1928). In this plot, the degree of pile-up and sink-in is represented by the normalized pile-up parameter s/h (see Fig. 1), where $s/h = c^2 - 1$. Also shown in the figure is the empirical relation suggested by Matthews (1980):

$$\frac{s}{h} = \frac{1}{2}\left(\frac{2+n}{2}\right)^{2(1-n)/n} - 1, \tag{2}$$

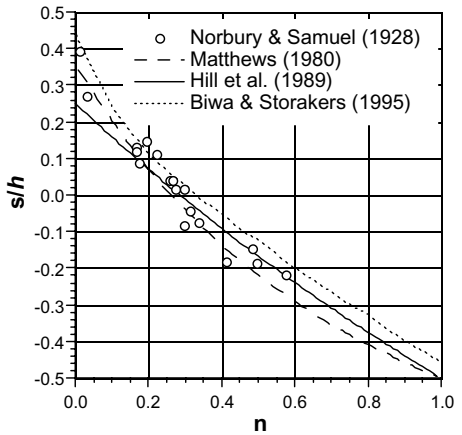

Fig. 2. Experimental data of Norbury and Samuel (1928) showing the dependence of the pile-up parameter, s/h, on the strain-hardening exponent, n. Shown for comparison are the models developed by Matthews (1980), Hill et al. (1989), and Biwa and Storakers (1995).

which appears to provide a slightly better fit of the experimental data. The relatively good agreement between theory and experiment suggests that pile-up and sink-in in the fully plastic regime can indeed be uniquely related to the strain hardening exponent, n.

The fact that the amount of pile-up and sink-in in the limit of fully plastic behavior depends only on the strain hardening exponent is a useful result for those interested in measuring mechanical properties by load and depth sensing indentation methods since it provides a means by which the contact area can be corrected for the influences of pile-up. For example, the observations in Fig. 2 form the basis of an approach developed by Field and Swain (1995) for measuring stress–strain curves and strain hardening exponents directly from load and depth sensing spherical indentation data. However, approaches like these ignore the fact that a significant portion of the data in a spherical indentation experiment can be in the elastic–plastic transition regime, for which fully plastic analyses may not apply.

In this work, the finite element method is used to explore and characterize the evolution of pile-up in the elastic–plastic transition. The approach adopted is similar to that used by Mesarovic and Fleck (1999), but with the specific objective of providing greater detail about the pile-up/sink-in behavior rather than describing the spherical indentation process in general. It is shown that the amount of pile-up and sink-in changes significantly during the elastic–plastic transition in a manner that depends on the elastic and the plastic properties of the material. Furthermore, although the behavior at large penetration depths approaches that predicted in the analyses of Hill et al. and Biwa and Storakers, the transition over which the pile-up height changes extends to much greater depths than would be expected based on normal indicators of the onset of full plasticity. Important effects of frictions are identified, and it is shown that there can be significant changes in the pile-up geometry after unloading. Collectively, the observations suggest that the influences of pile-up on spherical indentation are quite complex and not well-suited to correction by methods based on fully plastic analyses. The practical implications for load and depth sensing indentation testing are discussed.

2. Finite element simulation

Simulation of the spherical indentation process was performed using the ABAQUS® finite element (FE) code. As shown in Fig. 3, an axisymmetric formulation was employed using a cylindrical coordinate system with radial coordinate, r, and axial coordinate, z. The indenter was modeled as a rigid sphere of radius $R = 1$–50 mm, depending on the indentation regime of interest, and the specimen as a cylinder 20 mm in radius and 20 mm in height discretized into 1746 linear four-node elements. The indentation depth and indenter radius were coordinated so that the contact radius never exceeded 1 mm. Roller boundary conditions were applied at the bottom surface by enforcing no displacements in the z direction and free movement in the r direction. Symmetry boundary conditions were applied along the centerline, and a free surface was modeled at the outside of the specimen and on the top surface outside the region of contact. In most computations, a friction coefficient $\mu = 0.2$ was used to describe the interface between the indenter and the specimen, although in a limited number of simulations the influences of friction were examined using $\mu = 0.0$, 0.1, 0.2, and 1.0.

Fig. 4 shows the assumed elastic–plastic constitutive law. Linear elastic behavior with Young's modulus E and Poisson's ratio $\nu = 0.3$ was assumed up to the yield stress σ_y. Thereafter, the behavior was modeled as elastic–plastic with power-law hardening of the normal form $\sigma = K\varepsilon^n$. To assure continuity at the yield point, the strength coefficient, K, was related to the other material parameters through $K = \sigma_y/(\sigma_y/E)^n$ (see Fig. 4). A strain rate independent model based on Mises flow theory with isotropic hardening was used in all computations.

The pile-up/sink-in behavior was systematically characterized in the way it depends on the normalized depth of penetration, h/R, the ratio of the modulus to the yield strength, E/σ_y, the strain hardening

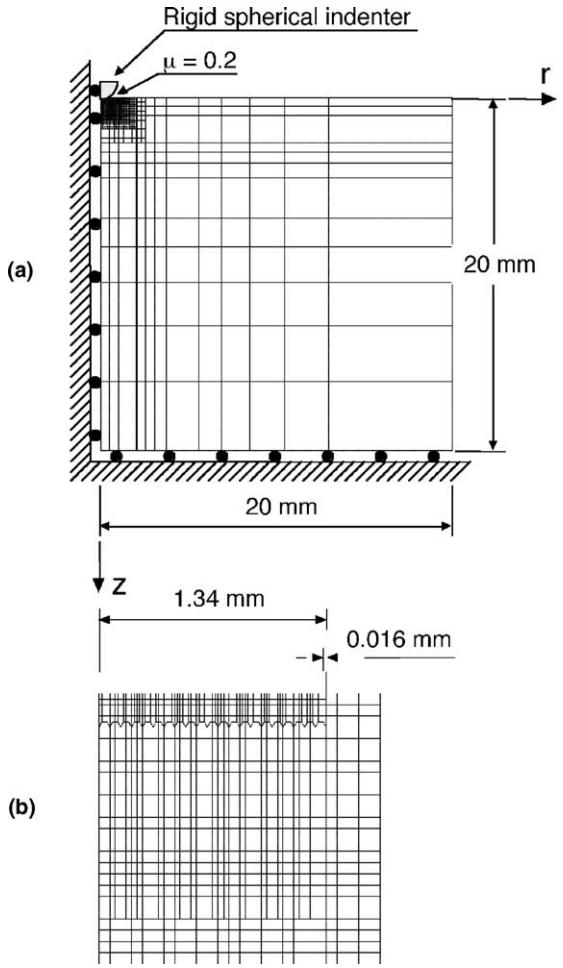

Fig. 3. The finite element mesh: (a) overall; (b) detail in the region of contact.

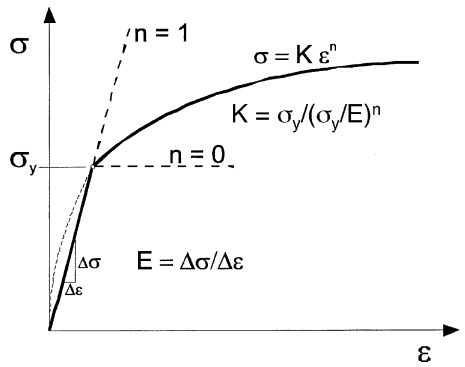

Fig. 4. A schematic representation of the elastic–plastic constitutive law used in the finite element simulations.

exponent, n, and the friction coefficient, μ. To cover a wide variety of elastic–plastic materials, values of E/σ_y were varied over the range $20 \leqslant E/\sigma_y \leqslant 1500$, which covers most metals, ceramics, and glasses. An ideal elastic material ($E/\sigma_y \to 0$) and a rigid-plastic material ($E/\sigma_y \to \infty$) were also examined to establish important limits. Simulations were performed for elastic–perfectly-plastic materials ($n = 0$) as well as strain hardening materials with $n = 0.25$ and 0.5. Throughout the work, both loaded and unloaded indentations were examined to establish how the pile-up geometry changes when the indenter is withdrawn. The computed parameters of interest included the contact radii, a_c and a, the contact depth, h_c, the pile-up/sink-in height, s, the load, P, and the contact profile geometry (see Fig. 1).

3. Results and discussion

3.1. Influence of elastic deformation on pile-up

How the pile-up evolves during the course of spherical indentation is strongly dependent on the relative amounts of elastic and plastic deformation as characterized by the ratio of the elastic modulus to yield stress, E/σ_y. Johnson (1970, 1985) noted that this parameter physically represents the reciprocal of the elastic strain at yielding and can therefore be used as a measure of the amount of deformation that is accommodated elastically during indentation. In the limit $E/\sigma_y = 0$, contact is strictly elastic and dominated by sink-in in the manner prescribed by Hertzian contact mechanics (Hertz, 1896). At the other extreme, the limit $E/\sigma_y = \infty$ corresponds to rigid-plastic deformation, for which there is extensive pile-up of material around the hardness impression (Hill et al., 1989; Biwa and Storakers, 1995). The intervening elastic–plastic behavior was examined by finite element simulation.

Fig. 5 shows finite element predictions of indentation profiles under load for several different materials deformed to the same normalized penetration depth $h/R = 0.2$ and a friction coefficient $\mu = 0.2$. The materials were a purely elastic solid, a rigid/perfectly-plastic solid, and three elastic/plastic solids with $E/\sigma_y = 20$, 100, and 1000 and no strain hardening ($n = 0$). Sink-in is observed in the elastic material as well as the elastic/plastic material with $E/\sigma_y = 20$. The material with $E/\sigma_y \approx 100$ exhibits a small amount of pile-up, while pile-up is extensive for the material with $E/\sigma_y = 1000$. After unloading, the contact geometry changes due to elastic recovery, as shown in Fig. 6. In order to make this figure directly comparable to Fig. 5, the values of h and a at full load were used to normalize the unloaded profiles. As expected, the purely

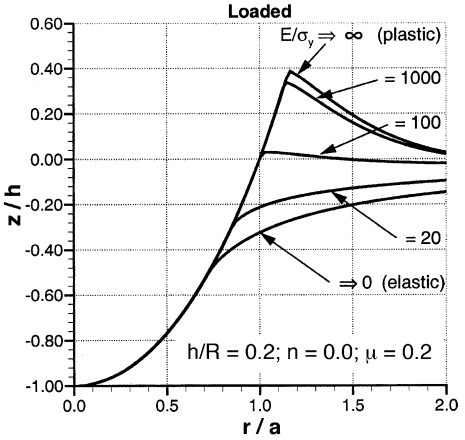

Fig. 5. Loaded indentation profiles for $h/R = 0.2$, $n = 0$, and $\mu = 0.2$ showing the influence of E/σ_y on the pile-up/sink-in behavior.

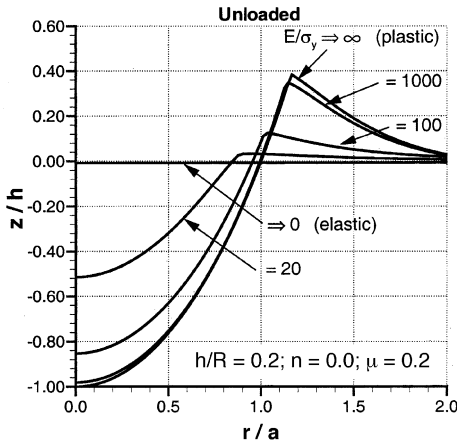

Fig. 6. Indentation profiles for $h/R = 0.2$, $n = 0$, and $\mu = 0.2$ corresponding to those in Fig. 5 after unloading. To facilitate comparison to Fig. 5, values of h and a at full load were used to normalize the axes.

elastic material recovers completely. Recovery is also large for the material with $E/\sigma_y = 20$, but there is little recovery for the material with $E/\sigma_y = 1000$ due to the fact that deformation at these strains is dominated by plasticity.

Fig. 7 shows how the normalized pile-up parameter s/h varies with E/σ_y for $h/R = 0.2$ and $\mu = 0.2$. For loaded indentations in purely elastic materials ($E/\sigma_y = 0$), the pile-up parameter is -0.5, in agreement with Hertzian contact mechanics. With increasing E/σ_y, the value rises to $s/h = 0$ at $E/\sigma_y \approx 100$, becomes positive for materials with higher E/σ_y, and reaches a nearly constant value when $E/\sigma_y \approx 1000$. For rigid/plastic materials ($E/\sigma_y = \infty$), $s/h = 0.38$ in relatively good agreement with the predictions of Hill et al. (1989) and Matthews (1980). After unloading, $s/h = 0$ for elastic materials ($E/\sigma_y = 0$) but grows larger with increasing E/σ_y. In the limit of rigid-plastic behavior ($E/\sigma_y = \infty$), there is no elastic recovery and s/h remains unchanged at 0.38.

Collectively, these observations demonstrate that: (1) the pile-up/sink-in geometry depends of the relative amounts of elastic and plastic deformation as determined by the value of E/σ_y, and (2) due to elastic

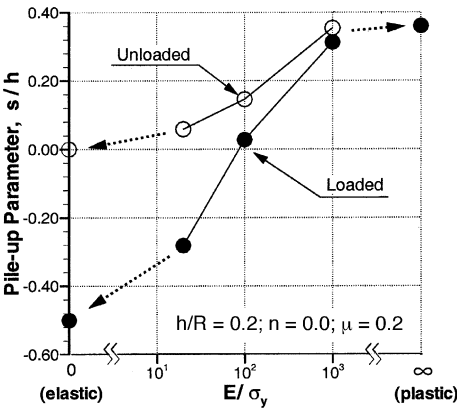

Fig. 7. Dependence of the pile-up parameter, s/h, on E/σ_y for $h/R = 0.2$, $n = 0$, and $\mu = 0.2$. Data for loaded and unloaded indentations are included.

recovery, the geometry of loaded and unloaded contact impressions may be very different, especially for smaller values of E/σ_y.

3.2. Dependence of pile-up on penetration depth

Fig. 8 shows how the pile-up and sink-in behavior depends on the normalized penetration depth h/R for elastic/perfectly-plastic materials ($n = 0$; $\mu = 0.2$). To capture measurable amounts of both sink-in and pile-up, the simulations were performed for a material with $E/\sigma_y = 200$. At small depths, the material deforms only elastically, and the indentation profile corresponds to that of Hertzian contact with $s/h = -0.5$. First yielding occurs at $h/R \approx 1.4 \times 10^{-4}$ and a mean pressure $p_m \approx 1.1\sigma_y$ in a region in the material on the axis of symmetry below the surface at $z \approx 0.5a_c$, also in accordance with Hertzian contact theory (see Tabor, 1951). As the load on the indenter is increased, the plastic zone grows and spreads upward, and the sink-in diminishes. At h/R of about 0.08, material starts to pile-up, and with further penetration, the pile-up becomes larger.

Fig. 9 shows the indentation profiles after unloading. In addition to the normalized depths h/R at which the profiles were determined, the figure also includes the values of the normalized surface radii a/R in order to provide a sense of the radial extent of the contact. The largest contact, $h/R = 0.34$, corresponds to $a/R = 0.75$ and thus a contact radius that is 75% of the indenter radius. As expected, full elastic recovery is observed when $h/R \leqslant 1.4 \times 10^{-4}$. For greater depths, the extent of the recovery diminishes with increasing h/R, and the residual contact impression always exhibits some pile-up.

Fig. 10 compares the depth dependence of the pile-up parameter s/h in both the loaded and unloaded conditions. Although the two curves converge at large depths, it is clear that the loaded and unloaded indentations can be very different due to elastic recovery, especially when $h/R < 0.1$. It is also notable that an upper limiting value for s/h is not reached at the maximum depth of penetration ($h/R = 0.34$ and $a/R = 0.75$). This is important because it shows that the pile-up geometry can continue to change significantly even up to contact radii in excess of $0.75R$, a value near the upper end of most indentation experiments. Thus, in addition to its dependence on E/σ_y, the pile-up height is a strong function of the depth of penetration.

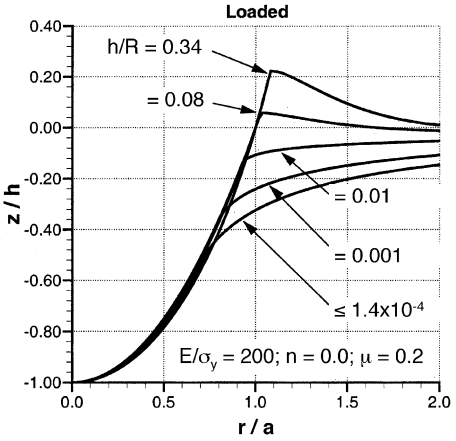

Fig. 8. Loaded indentation profiles for $E/\sigma_y = 200$, $n = 0$, and $\mu = 0.2$ showing the influence of the normalized penetration depth, h/R, on the pile-up/sink-in behavior.

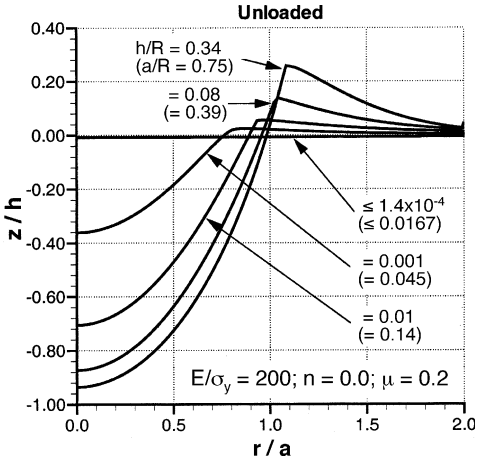

Fig. 9. Indentation profiles for $E/\sigma_y = 200$, $n = 0$, and $\mu = 0.2$ corresponding to those in Fig. 8 after unloading. To facilitate comparison to Fig. 8, values of h and a at full load were used to normalize the axes.

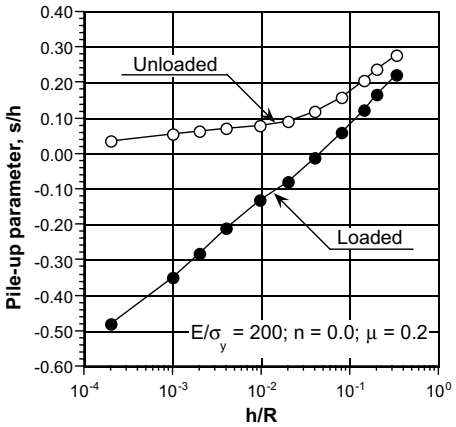

Fig. 10. Dependence of the pile-up parameter, s/h, on the normalized penetration depth, $h/2R$, for $E/\sigma_y = 200$, $n = 0$, and $\mu = 0.2$. Data for loaded and unloaded indentations are included.

3.3. Dependence of pile-up on contact friction

Contact friction can also affect the pile-up behavior, especially in materials with large E/σ_y and small n. The effects of friction are demonstrated in Fig. 11, which shows loaded indentation profiles at $h/R = 0.2$ for four different friction coefficients: $\mu = 0.0$, 0.1, 0.2, and 1.0. The plot includes data for an elastic/perfectly-plastic material with $E/\sigma_y = 1000$ and $n = 0$ and an elastic/strain-hardening-plastic material with $E/\sigma_y = 1000$ and $n = 0.5$. Clearly, frictional effects are most important in materials that do not strain harden; there is a strong tendency for pile-up to develop in these materials, and friction acts to reduce it. On the other hand, for strongly hardening materials ($n = 0.5$), there is no discernable effect of friction, but there is also no tendency to pile-up. The reason that pile-up is diminished in strain-hardening materials is that localized hardening near the contact periphery impedes plasticity near the surface, driving the plastic zone deeper into the material rather than radially outward.

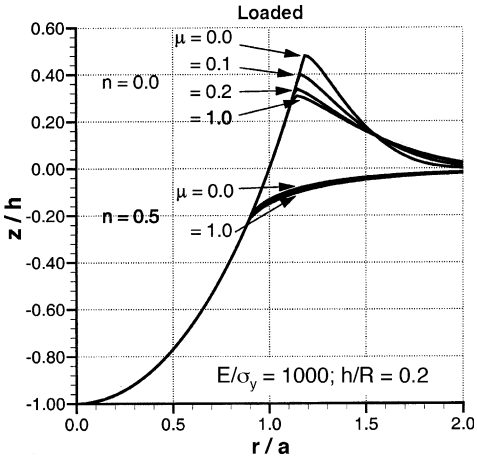

Fig. 11. Effect of contact friction on the indentation profile for $h/R = 0.2$, $E/\sigma_y = 1000$, and $n = 0.0$ and 0.5.

3.4. Combined effects of elasticity and depth of penetration

Comparison of Figs. 5 and 8 reveals some important similarities about the effects of elasticity and the depth of penetration on the pile-up behavior, specifically, increasing h/R is qualitatively similar to increasing E/σ_y. This is not just mere coincidence but results from the fact that both parameters are related to the relative amount of elastic and plastic deformation during contact. Deformation is largely elastic when E/σ_y and h/R are small, but becomes more plastic as they increase. In this sense, one might expect that the two parameters could be combined into a single parameter that provides a unified description of the pile-up behavior. A natural choice is $E/\sigma_y \tan\beta$, as used by Johnson to correlate the constraint factor p_m/σ_y with material parameters and the contact geometry. In such a description, the depth dependence is embodied in the way that β increases with h/R (see Fig. 1). To explore this possibility, the dependence of the pile-up parameter s/h for two extreme elastic–perfectly-plastic materials ($E/\sigma_y = 20$ and 2000) is plotted in Fig. 12 as a function of two parameters that approximate to $E/\sigma_y \tan\beta$ but can be estimated from indentation load and depth data. The parameters are: (1) $\tan\beta \cong a_c/R$, and (2) $\tan\beta \cong 2h_c/a_c$. The former is a first-order approximation often used to describe spherical indentation at small depths. The latter is a second-order approximation that is more accurate at larger depths. The plot shows that the pile-up data

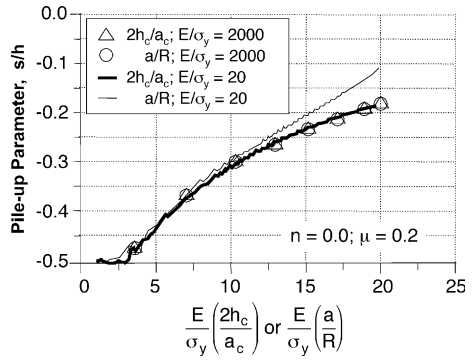

Fig. 12. The correlation of the pile-up parameter, s/h, with the parameters $(E/\sigma_y)(2h_c/a_c)$ and $(E/\sigma_y)(a/R)$.

converge remarkably well when $(E/\sigma_y)(2h_c/a_c)$ is used as the unifying parameter. The parameter $(E/\sigma_y)(a_c/R)$ also provides a reasonable approximation, but it is not as good as $(E/\sigma_y)(2h_c/a_c)$ when E/σ_y is small and a_c/R is large.

Note that in a formal sense, the modulus E used in the plotting parameters should be the plane strain modulus $E^* = E/(1-\nu^2)$ (Johnson, 1985) rather than Young's modulus, E. For the value $\nu = 0.3$ used in all the finite element calculations, E^* is slightly higher than E (about 10%), and the plotting parameters should be adjusted accordingly if the Poisson effect is to be included.

3.5. Influences of strain hardening

The use of $(E/\sigma_y)(2h_c/a_c)$ as a unifying parameter was found to work equally well for strain hardening materials. Fig. 13 summarizes the observed correlations between s/h and $(E/\sigma_y)(2h_c/a_c)$ for materials with $\mu = 0.2$ and strain hardening exponents $n = 0.0$, 0.25, and 0.50. The filled plotting symbols represent the pile-up parameter when the indenter is fully loaded and the open symbols the behavior after unloading. The results were obtained in a series of simulations in which E/σ_y was varied systematically from 20 to 1500 and R from 1 to 50 mm, so that s/h was calculated over the range $1 \leqslant (E/\sigma_y)(2h_c/a_c) \leqslant 1000$. The curves are composites of the unified behavior observed for each value of n. For materials with small E/σ_y, some deviation was observed at large depths, where the curves peaked and exhibited a downturn prior to reaching the relatively constant value at $(E/\sigma_y)(2h_c/a_c) > 1000$. Mesarovic and Fleck (1999), who examined this behavior in detail, attributed it to a combination of elastic influences and finite deformation effects at large strain that cannot be accounted for in the plastic analysis of Hill et al. (1989). Because of this, caution should be exercised in applying the results in Fig. 13 to situations of large h/R at small E/σ_y. The work of Mesarovic and Fleck (1999) should be consulted to provide guidelines as to when these effects may be important.

A number of features in Fig. 13 are worthy of note. First, at small $(E/\sigma_y)(2h_c/a_c)$, the behavior is independent of strain hardening because the material deforms only elastically. Loaded indentations sink-in to $s/h = -0.5$, as predicted by Hertzian contact mechanics, and the indentations fully recover after unloading giving $s/h = 0$. Plasticity commences at $(E/\sigma_y)(2h_c/a_c) \approx 2.5$, also as predicted by Hertzian mechanics, but even then there is essentially no dependence on strain hardening because yielding begins well beneath the surface and the initial stages of plastic deformation are highly constrained by the surrounding elastic material. Only when the plasticity breaks through to the surface at $(E/\sigma_y)(2h_c/a_c) \approx 10$ do strain

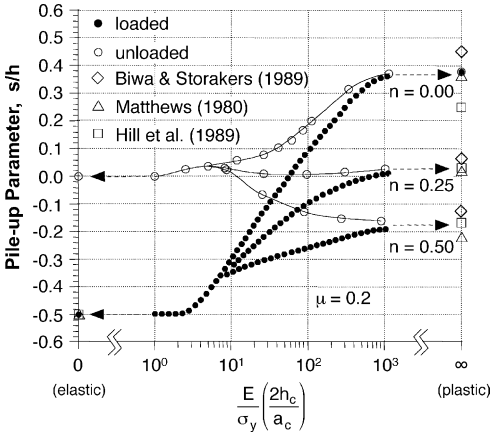

Fig. 13. Dependence of the pile-up parameter, s/h, on $(E/\sigma_y)(2h_c/a_c)$ for $\mu = 0.2$ and $n = 0$, 0.25, and 0.5. Data for loaded and unloaded indentations are included.

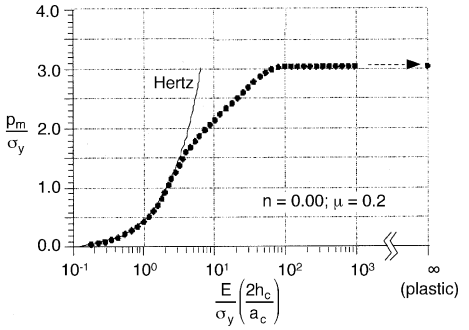

Fig. 14. Dependence of the normalized mean contact pressure, p_m/σ_y, on $(E/\sigma_y)(2h_c/a_c)$ for elastic–perfectly-plastic materials with $n = 0$ and $\mu = 0.2$.

hardening effects become apparent. Thereafter, the pile-up grows in a manner that depends on the strain hardening exponent, with larger pile-up produced in materials with smaller n. The pile-up is fully developed and s/h ceases to increase only when $(E/\sigma_y)(2h_c/a_c) > 1000$. The values of s/h in the rigid-plastic limit $[(E/\sigma_y)(2h_c/a_c) \to \infty]$ are consistent with the models of Hill et al. (1989), Biwa and Storakers (1995), and Matthews (1980), data points for which are included at the rigid-plastic limit at the right-hand side of the plot. Note that there is large pile-up for $n = 0$, sink-in predominates for $n = 0.5$, and materials with $n = 0.25$ show neither pile-up nor sink-in. These observations are in agreement with the analysis of Hill et al. (1989) which shows that the cross-over from sink-in to pile-up should occur at $n = 0.22$.

Another noteworthy feature in Fig. 13 concerns the fact that pile-up is not fully developed until $(E/\sigma_y)(2h_c/a_c) \approx 1000$. This is particularly interesting when compared to the data in Fig. 14, which shows the corresponding development of the constraint factor, p_m/σ_y, for a material with $n = 0$. Fig. 14 suggests that fully developed plasticity, as conventionally defined by the point at which the constraint factor levels off at a value of about 3, commences at the much smaller value $(E/\sigma_y)(2h_c/a_c) \approx 100$. Thus, the pile-up geometry continues to change well after the traditional beginning of full plasticity, and one cannot use the observation of a relatively constant constraint factor as an indication that pile-up is also fully developed. To help further illustrate this point, it is useful to consider some typical numbers. For $E/\sigma_y = 10$, 100, and 1000, the contact depths at which $(E/\sigma_y)(\tan\beta) = 1000$ are 99%, 90%, and 29% of the sphere radius, respectively. Thus, fully developed pile-up consistent with the predictions of plasticity theory is experimentally achievable only in materials with very large E/σ_y, i.e., the softer metals. For other materials, the pile-up geometry can be expected to change continuously during the course of an indentation experiment. Although not explicitly noted, this same behavior is also observed in the finite element results of Mesarovic and Fleck (1999).

Another important observation in Fig. 13 concerns the pile-up geometry after unloading. The results indicate that over a considerable range of $(E/\sigma_y)(2h_c/a_c)$, the pile-up before and after unloading can be greatly different due to elastic recovery. Thus, analysis of residual contact geometries based on models for rigid-plastic behavior may not be appropriate for materials with smaller E/σ_y. Moreover, functional relationships for s/h developed from observations of residual hardness impressions may not apply to load and depth sensing indentation experiments, for which indentations are analyzed primarily in the loaded condition.

3.6. Implications for load and depth sensing indentation

The primary objective of this work is to give investigators who measure mechanical properties by load and depth sensing indentation techniques some insight into the amount of pile-up or sink-in that can be expected at various points in the spherical indentation process. In principle, this can be accomplished from

the data in Fig. 13 if one has some idea of the material parameters E/σ_y and n. However, estimation of the pile-up parameter is not necessarily straightforward, since the independent parameter $2h_c/a_c$ used in Fig. 13 is not directly measurable in load and depth sensing experiments. To rectify this, it is suggested that a first estimate of the pile-up or sink-in behavior can be obtained by approximating $2h_c/a_c$ with $2h/a$, which can be determined from the total measured depth, h, and the geometric relation $a = \sqrt{2Rh - h^2}$. Considering the limiting cases of purely elastic deformation with maximum sink-in ($s/h = -0.5$), and rigid–perfectly-plastic behavior with maximum pile-up ($s/h = 0.36$), simple geometric considerations show that 2h/a deviates from $2h_c/a_c$ by no more than a factor of 1.5, with the two being much closer under most circumstances. Because the abscissa in Fig. 13 is logarithmic, differences of a factor of 1.5 are not particularly significant in their effect on s/h. Thus, an approximation of the pile-up or sink-in can be obtained from Fig. 13 by using $2h/a$ to approximate $2h_c/a_c$.

4. Conclusions

Finite element simulations have shown that pile-up and sink-in during spherical indentation of elastic–plastic materials depend not only on the strain hardening exponent, n, as is often used to model and analyze load and depth sensing indentation data, but also on the relative amount of elastic and plastic deformation as characterized by the non-dimensional material parameter E/σ_y, the non-dimensional depth of penetration, h/R, and the friction coefficient, μ. The dependencies of the pile-up parameter, s/h, on E/σ_y and h/R can be conveniently described by the single parameter $(E/\sigma_y)(2h_c/a_c)$ which approximates to the quantity $E/\sigma_y \tan\beta$ used by Johnson to divide indentation into elastic, elastic–plastic transition, and fully plastic regimes. In the elastic regime, sink-in is observed in a manner consistent with Hertzian contact mechanics. During the elastic–plastic transition, the pile-up grows in a way that depends on the strain hardening exponent and friction coefficient. The pile-up parameter s/h becomes constant and pile-up is fully developed only when $(E/\sigma_y)(2h_c/a_c) > 1000$, well beyond the value $(E/\sigma_y)(2h_c/a_c) \approx 100$ that marks the traditional beginning of the fully plastic regime based on a constant constraint factor $p_m/\sigma_y \approx 3$. Thus, in many materials, the pile-up geometry can be expected to change continuously during the course of a spherical indentation experiment, and it is not appropriate to use results obtained from fully plastic analyses to model it.

Due to elastic recovery, the amount of pile-up depends on whether it is measured with the indenter loaded or unloaded. Elastic recovery is especially important at small depths of penetration and in materials with small E/σ_y. Thus, when recovery is large, descriptions of pile-up based on measurements of residual hardness impressions may not be appropriate for analyzing load and depth sensing indentation data since load and depth sensing measurements usually apply to the fully loaded state.

Friction affects pile-up in a manner that depends on strain hardening exponent, n. For $n = 0$, friction reduces the amount of pile-up by as much as 50%. For $n = 0.5$, sink-in predominates at all stages of indentation, and friction effects are negligible.

Collectively, these observations show that the development of pile-up and sink-in during spherical indentation is a complex phenomena that is not amenable to simple analytical descriptions. The finite element results summarized in the plot of s/h vs. $(E/\sigma_y)(2h_c/a_c)$ in Fig. 13 may be used as a first estimate of the pile-up/sink-in behavior if the material parameters E/σ_y and n are known.

Acknowledgements

Research at the Oak Ridge National Laboratory was sponsored by the Division of Materials Sciences and Engineering, US Department of Energy, under contract DE-AC05-00OR22725 with UT-Battelle, LLC.

References

Biwa, S., Storakers, B., 1995. An analysis of fully plastic Brinell indentation. Journal of Mechanics and Physics of Solids 43 (8), 1303–1333.

Bolshakov, A., Pharr, G.M., 1998. Influences of pile-up on the measurement of mechanical properties by load and depth sensing indentation techniques. Journal of Materials Research 13 (4), 1049–1058.

Field, J.S., Swain, M.V., 1995. Determining the mechanical properties of small volumes of material from submicron spherical indentations. Journal of Materials Research 10 (1), 101–112.

Francis, H.A., 1976. Phenomenological analysis of plastic spherical indentation. Transactions of the ASME Journal of Engineering Materials and Technology (July), 272–281.

Hertz, H., 1896. Miscellaneous Papers by H. Hertz. Macmillan, London.

Hill, R., Storakers, B., Zdunek, A.B., 1989. A theoretical study of the Brinell hardness test. Proceedings of the Royal Society of London A 423, 301–330.

Johnson, K.L., 1970. The correlation of indentation experiments. Journal of the Mechanics and Physics of Solids 18, 115–126.

Johnson, K.L., 1985. Contact Mechanics. Cambridge University Press, Cambridge, UK.

Matthews, J.R., 1980. Indentation hardness and hot pressing. Acta Metallurgica 28, 311–318.

Mesarovic, S.D.J., Fleck, N.A., 1999. Spherical indentation of elastic–plastic solids. Proceedings of the Royal Society of London A 455, 2707–2728.

Norbury, A.L., Samuel, T., 1928. The recovery and sinking-in or piling-up of material in the Brinell test, and the effect of these factors on the correlation of the Brinell with other hardness tests. Journal of the Iron and Steel Institute 117, 673–687.

Oliver, W.C., Pharr, G.M., 1992. An improved technique for determining hardness and elastic modulus using load and displacement sensing indentation techniques. Journal of Materials Research 7 (6), 1564–1583.

O'Neil, H., 1944. The significance of tensile and other mechanical test properties of metals. Proceedings of the Institute of Mechanical Engineers 151, 116–130.

Pharr, G.M., 1998. Measurement of mechanical properties by ultra-low load indentation. Materials Science and Engineering A 253, 151–159.

Tabor, D., 1951. The Hardness of Metals. Clarendon Press, Oxford, UK.